www.nature.com/scientificreports

SCIENTIFIC REPORTS

OPEN

Urban heat island impacted by fine particles in Nanjing, China

Hao Wu[1], Tijian Wang[1], Nicole Riemer[2], Pulong Chen[1], Mengmeng Li[1] & Shu Li[1]

Received: 16 May 2017
Accepted: 29 August 2017
Published online: 12 September 2017

Atmospheric aerosol particles (especially particles with aerodynamic diameters equal to or less than 2.5 μm, called $PM_{2.5}$) can affect the surface energy balance and atmospheric heating rates and thus may impact the intensity of urban heat islands. In this paper, the effect of fine particles on the urban heat island intensity in Nanjing was investigated via the analysis of observational data and numerical modelling. The observations showed that higher $PM_{2.5}$ concentrations over the urban area corresponded to lower urban heat island (UHI) intensities, especially during the day. Under heavily polluted conditions, the UHI intensity was reduced by up to 1 K. The numerical simulation results confirmed the weakening of the UHI intensity due to $PM_{2.5}$ via the higher $PM_{2.5}$ concentrations present in the urban region than those in the suburban areas. The effects of the fine particles on the UHI reduction were limited to the lowest 500–1000 m. The daily range of the surface air temperature was also reduced by up to 1.1 K due to the particles' radiative effects. In summary, $PM_{2.5}$ noticeably impacts UHI intensity, which should be considered in future studies on air pollution and urban climates.

The term urban heat island (UHI) refers to the increased surface temperatures in urban centres compared to those of their suburban surroundings. The phenomenon was first observed in London[1] and was named by Manley[2]. The UHI phenomenon is a result of the differences in the surface roughnesses, surface albedos, anthropogenic activities and building densities between an urban centre and its suburban surroundings[3–5], which cause differences in the local boundary layer characteristics and the underlying surface energy balance[6,7]. For example, during the day, urban centres experience sensible heat convection efficiency reductions because urban areas are aerodynamically smoother than their surrounding suburban regions[8]. As such, the local UHI effect is distinct from large-scale global warming trends[9–11].

The approaches for quantifying a UHI phenomenon include in situ observations[9,12,13] and remote sensing[4] as well as numerical modelling[6], all of which typically compare a climate indicator, such as the surface air temperature, between a location representing an urban environment and another location representing a suburban environment. Previous studies found that UHIs are more pronounced at night than during the day and are larger in the winter than in the summer[14].

Several studies have recognized the impacts of UHIs on local meteorology and air quality. Differential heating produces mesoscale winds, which help pollutants circulate and move upward, leading to air pollution issues in urban areas[15]. Thus, UHIs also have significant effects on pollutant concentrations, such as those of ozone and particles, due to their feedbacks on boundary layer stability, which decreases the intensity of vertical mixing[16–18].

Urban centres are also the dominant sources of fine particles, which have important impacts on boundary layer development via their reduction of the amount of solar radiation reaching the earth surface. This reduction affects the surface radiation balance, leading to a decrease in the surface temperature[19,20]. Numerical models have been used to quantify the radiative effects of aerosol particles. For example, the regional chemistry climate model COSMO-ART has been used in aerosol-climate studies over Europe[21]. This study found a correlation between the aerosol optical depths and changes in regional temperatures. Im *et al.*[22] concluded that small differences in summer $PM_{2.5}$ levels can cause changes in temperature of 1.5–4.5 K. The chemical speciation of $PM_{2.5}$ matters in this context as it determines whether the particles only scatter light or also absorb light; sulfate aerosols have a strong cooling effect due to their scattering characteristics, which cause the surface temperatures to decrease as sulfate concentrations increase[23–25]. In contrast, the presence of black carbon may reduce the aerosol cooling effect since this particle is the main absorbing component in anthropogenic aerosols[26]. A large black carbon column burden

[1]School of Atmospheric Sciences, CMA-NJU Joint Laboratory for Climate Prediction Studies, Jiangsu Collaborative Innovation Center for Climate Change, Nanjing University, Nanjing, China. [2]Department of Atmospheric Sciences, University of Illinois at Urbana-Champaign, Urbana, USA. Correspondence and requests for materials should be addressed to T.W. (email: tjwang@nju.edu.cn)

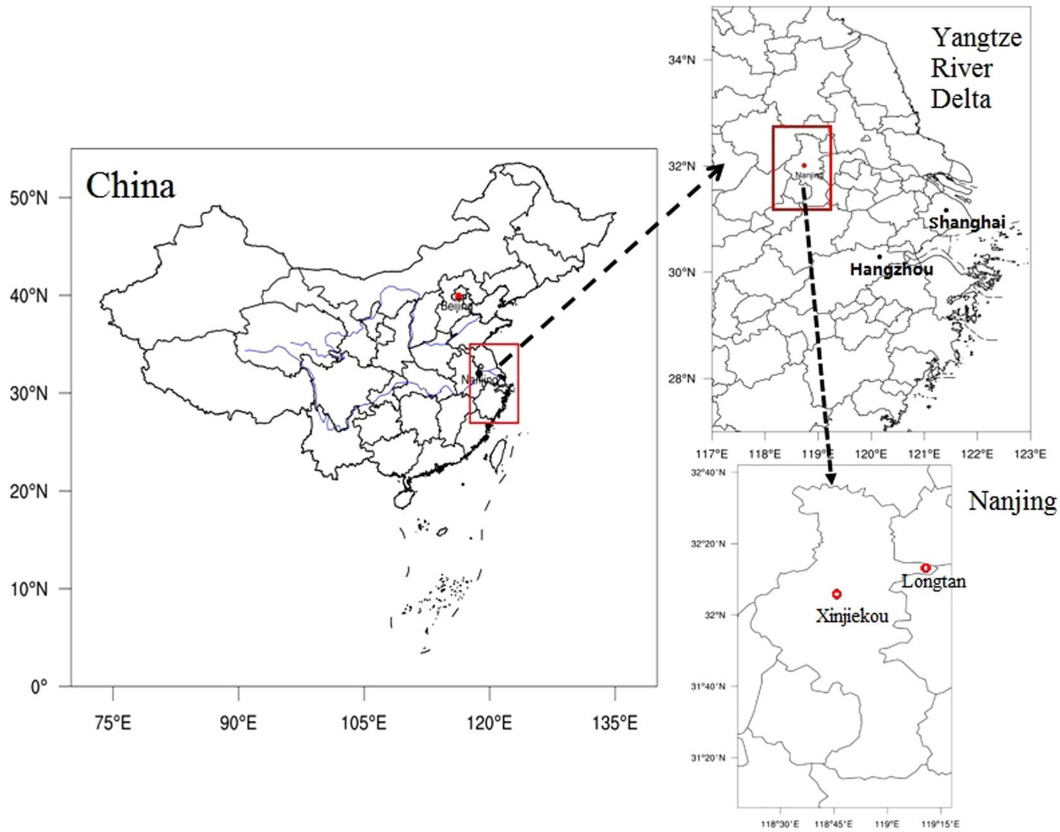

Figure 1. Locations of the urban station (Xinjiekou) and the suburban station (Longtan) in Nanjing, China. The maps were generated using the NCAR Command Language (Version 6.2.0., https://www.ncl.ucar.edu, 2014).

was found to decrease the surface temperature by nearly 2 K in eastern China while warming the atmosphere at the top of the boundary layer[27].

Although many investigations of fine particles' radiative forcing and climate effects exist, only a few studies have focused on the impacts of fine particles on UHIs. The radiative forcings of fine particles are different in urban and suburban regions due to the inherently different $PM_{2.5}$ loads[28], thus causing differences in the surface temperature cooling effects. Our previous study showed that the UHI intensity was weakened by 0.1–0.2 K during the day due to the impacts of fine particles, based on the surface energy balance equation[29]. However, Chang *et al.*[30] reported that the night-time UHI can be intensified due to increased incoming long-wave radiation, based on remote sensing temperature data from 39 cities in China.

This study uses one-year surface observations of $PM_{2.5}$ concentrations and temperatures as well as numerical modelling to investigate how UHIs could be affected by fine particles, taking Nanjing, a mega city with spreading urbanization located in the Yangtze River Delta of China, as the target city.

Methodology

Observational data. The study period spanned from 1st January to 31st December, 2011. The hourly surface temperature data were collected from the Nanjing Meteorological Bureau, and the hourly $PM_{2.5}$ concentration data came from the Nanjing Environmental Monitoring Center. The urban station is Beijige (118°48′37″ E, 31°59′59″N), while Pukou (118°36′7″E, 31°24′5″N) was selected as the suburban station. The Pukou station is situated in western Nanjing and is not influenced by mountains or the ocean. $PM_{2.5}$ was not widely observed in China before 2013. In 2011 in Nanjing, only one urban site produced $PM_{2.5}$ observations, and no suburban sites made $PM_{2.5}$ observations.

However, in 2014, $PM_{2.5}$ observations were available at both the urban site of Xinjiekou (118°47′26″E, 32°2′51″N) and the suburban site of Longtan (119°11′48″E, 32°11′58″N), both of which were used for the model experiments and have collocated surface temperature observation sites. We used these data to analyse the relationship between UHI intensities and the $PM_{2.5}$ concentration differences between the urban and suburban sites.

Numerical experiments. An online modelling system, the Weather Research and Forecasting (WRF) Model, coupled with Chemistry Version 3.5.1[31,32], was used to investigate the influences of fine particles on UHIs. The model system WRF-Chem uses a non-hydrostatic dynamical core and includes emissions of gas phase species and aerosols, gas phase chemical transformations, photolysis, aerosol chemistry and dynamics (including inorganic and organic aerosols) and the removal of gas phases and aerosol species by wet and dry deposition.

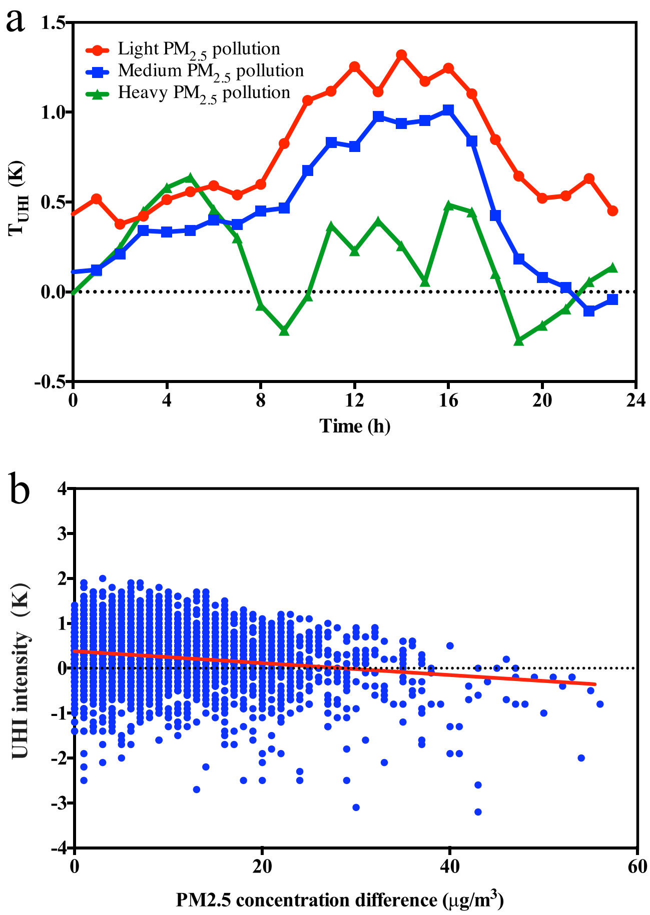

Figure 2. Observed correlations of UHI intensities and $PM_{2.5}$ concentration differences between the urban centre and the suburban station. (**a**) Observed diurnal variations of UHI intensities for different $PM_{2.5}$ levels in Nanjing, 2011. Red, blue and green lines indicate the UHI intensities with light pollution ($PM_{2.5} < 35\,\mu g/m^3$), medium pollution ($35\,\mu g/m^3 \leq PM_{2.5} \leq 75\,\mu g/m^3$) and heavy pollution ($PM_{2.5} > 75\,\mu g/m^3$), respectively. (**b**) Correlation between the observed UHI intensities and $PM_{2.5}$ concentration differences of Nanjing, 2014. Blue dots indicate the UHI intensities and the red line is the linear regression of the UHI intensity and the $PM_{2.5}$ concentration difference. The figure was produced using Prism 6.

The physics scheme in this study was PBL with YSU[33]. The shortwave radiation parameterization was from NASA Goddard[34], and the longwave parameterization was RRTM[35]. The chemical mechanism was RADM2 (Second Generation Regional Acid Deposition Model; Stockwell *et al.*[36]) with 158 reactions among the gas phases of 36 species. The MADE/SORGAM (Modal Aerosol Dynamics Model for Europe/Secondary Organic Aerosol Model; Ackermann *et al.*[37]; Schell *et al.*[38]) was used for the secondary inorganic and organic aerosols. The emission module included biogenic and anthropogenic contributions. Biogenic emissions were calculated online using Guenther's scheme[39, 40]. Anthropogenic emissions were supplied from an offline resource, based on the work of MEIC (*Multi-resolution Emission Inventory for China*, http://www.meicmodel.org/dataset-meic.html), which included the species SO_2, NO_X, CO, NH_3, NMVOC, $PM_{2.5}$, PM_{10}, BC, OC and CO_2.

The model was configured with four one-way nested domains using grid resolutions of 81 km, 27 km, 9 km, and 3 km. The initial meteorological fields and boundary conditions were from the NCEP global reanalysis data-set with a 1° × 1° resolution.

In the numerical experiments, Xinjiekou (118°47′26″E, 32°2′51″N) was chosen as the urban point, as shown in Fig. 1. Xinjiekou is in the central district of Nanjing, close to Beijige, and has no heavy industrial emission sources within 30 km. However, the station is close to major roads with heavy traffic and a large population aggregation. The suburban point is located in Longtan (119°11′48″E, 32°11′58″N), in an eastern district of Nanjing, nearly 40 km away from the city centre of Xinjiekou. Longtan is surrounded by crop fields and inhabited by a small population, similar to Pukou.

To investigate the impact of fine particles on UHI intensities, two sets of numerical experiments were performed for January (winter), April (spring), July (summer) and October (fall), 2011. In the first experiment, the direct and indirect effects of aerosols were disabled. The second experiment included the direct and indirect effects of aerosols. Therefore, the differences of the UHI intensities of the two experiments quantify the effects of $PM_{2.5}$ on the UHI.

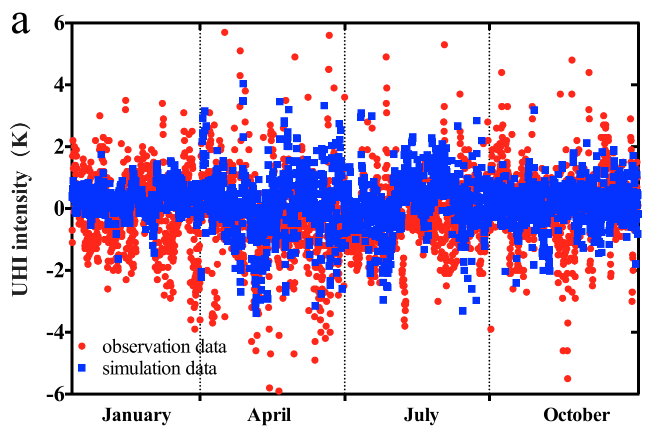

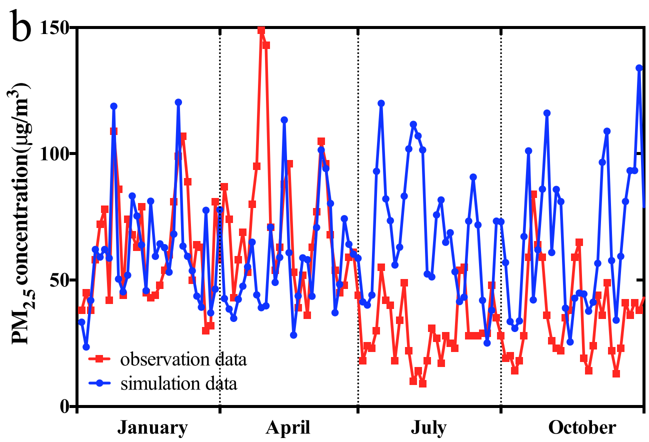

Figure 3. Comparison of observed and simulated UHI intensity and $PM_{2.5}$ concentration in Nanjing, 2011. (**a**) Comparison of hourly observed and simulated UHI intensities between the urban and suburban site. Red dots indicate observational data and blue dots indicate simulation data. (**b**) Comparison of the daily average observed and simulated $PM_{2.5}$ concentration data at the urban site. Red dots indicate the observational data and blue dots indicate the simulation data. The figure was produced using Prism 6.

In the following sections, the term surface UHI intensity, T_{UHI}, refers to the difference in the surface temperatures at the urban and suburban stations. The larger T_{UHI} is, the more intense the UHI effect. When investigating the $PM_{2.5}$ effect on UHI intensity, we define ΔT_{UHI} (the difference in T_{UHI} between the simulations with and without the $PM_{2.5}$ radiation effect) as the change in the UHI intensity due to the $PM_{2.5}$. A negative value of ΔT_{UHI} means that the UHI intensity is weakened by the presence of $PM_{2.5}$. We use the variable ΔT to represent the surface temperature changes including and excluding the $PM_{2.5}$ effect, with negative values of ΔT representing a lower surface temperature when $PM_{2.5}$ is present. The daily temperature range difference due to $PM_{2.5}$ is denoted by ΔT_{dr}.

Data availability. The data that support the findings of this study are available from the corresponding author upon reasonable request.

Results

Observed $PM_{2.5}$ effects on the UHI. Hourly surface air temperature data at the urban and suburban sites in Nanjing were used to estimate the hourly UHI intensities, T_{UHI}. To quantify the fine particles' effects on UHI intensities, we classified the hourly values of the UHI intensities into three groups according to the observed $PM_{2.5}$ concentrations in the urban area, representing light ($PM_{2.5}$ concentrations less than 35 μg/m^3), medium ($PM_{2.5}$ concentrations greater than or equal to 35 μg/m^3 and less than or equal to 75 μg/m^3) and heavy pollution ($PM_{2.5}$ concentrations greater than 75 μg/m^3).

Figure 2a compares the diurnal cycles of the T_{UHI} of the three pollution levels. The light and medium pollution levels show similar characteristics, with maximum values occurring during the afternoons (1.3 K and 1.1 K for light and medium pollution levels, respectively), and minimum values occurring at night (0.3 K and −0.1 K for light and medium pollution levels, respectively). As the pollution levels increase from light to medium, the UHI intensity decreases for all hours during the day by an average of 0.2 K.

The diurnal cycle of T_{UHI} for the heavy pollution case differs from the other two cases, as it does not exhibit a maximum in the afternoon. In contrast, for the heavy pollution case, T_{UHI} is larger at night and is approximately 1 K lower than the light and medium pollution cases during the day.

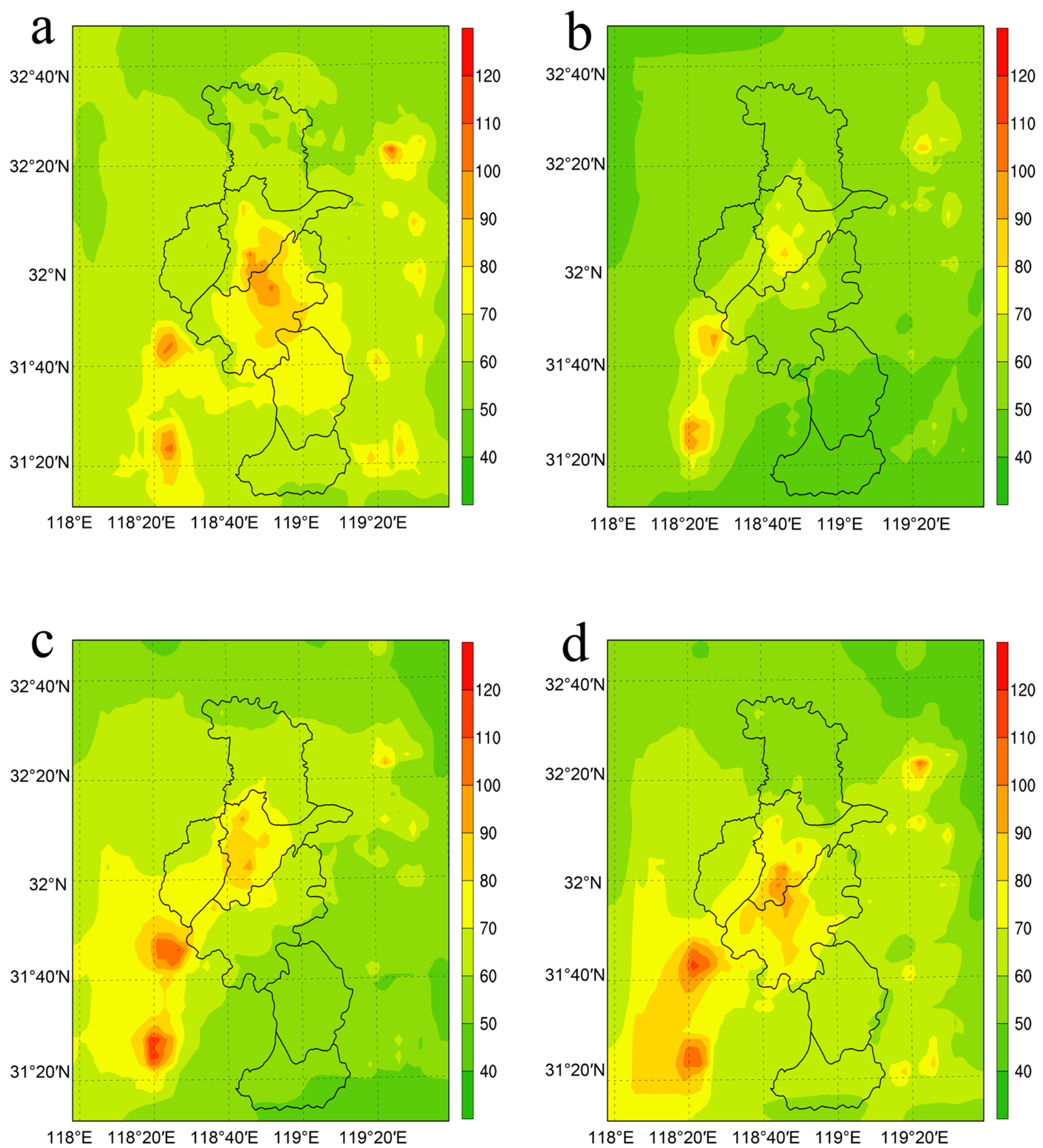

Figure 4. Monthly averaged simulated surface $PM_{2.5}$ concentrations (μg/m^3) for Nanjing. (**a**) January; (**b**) April; (**c**) July; (**d**) October, 2011. The maps were generated using NCAR Command Language (Version 6.2.0., https://www.ncl.ucar.edu, 2014).

Figure 2b shows the relationship between the UHI intensities and $PM_{2.5}$ concentration differences of the urban and suburban sites ($\Delta PM_{2.5}$) of Nanjing in 2014. Each data point represents an hourly value of a UHI intensity and the corresponding $PM_{2.5}$ concentration difference. The $PM_{2.5}$ levels at the urban site were always equal to or higher than those at the suburban site, with the differences ranging from 0 to 55 μg/m^3. A negative correlation between the UHI intensity and the $PM_{2.5}$ difference was found; as $\Delta PM_{2.5}$ increased, the UHI intensity tended to decrease.

Chang *et al.*[30] showed that $PM_{2.5}$ strengthened the UHI at night because it increased longwave radiation. Our results confirm this finding when we compare the light and medium $PM_{2.5}$ loadings to the heavy $PM_{2.5}$ loading. However, when comparing the light and medium $PM_{2.5}$ loading, we find a weakening of the UHI intensity for daytime and nighttime.

Simulated $PM_{2.5}$ effects on surface temperature. As described in the methodology section, WRF-Chem simulations were carried out to investigate the effects of $PM_{2.5}$ on the surface temperature. Two experiments, one with and one without the direct and indirect aerosol effects, were conducted. The differences of the surface temperatures of the two experiments were used to assess the role of $PM_{2.5}$ on the surface temperature. As fine particles have negative surface radiative forcings, we expect the surface temperatures to become cooler with higher $PM_{2.5}$ loadings[22].

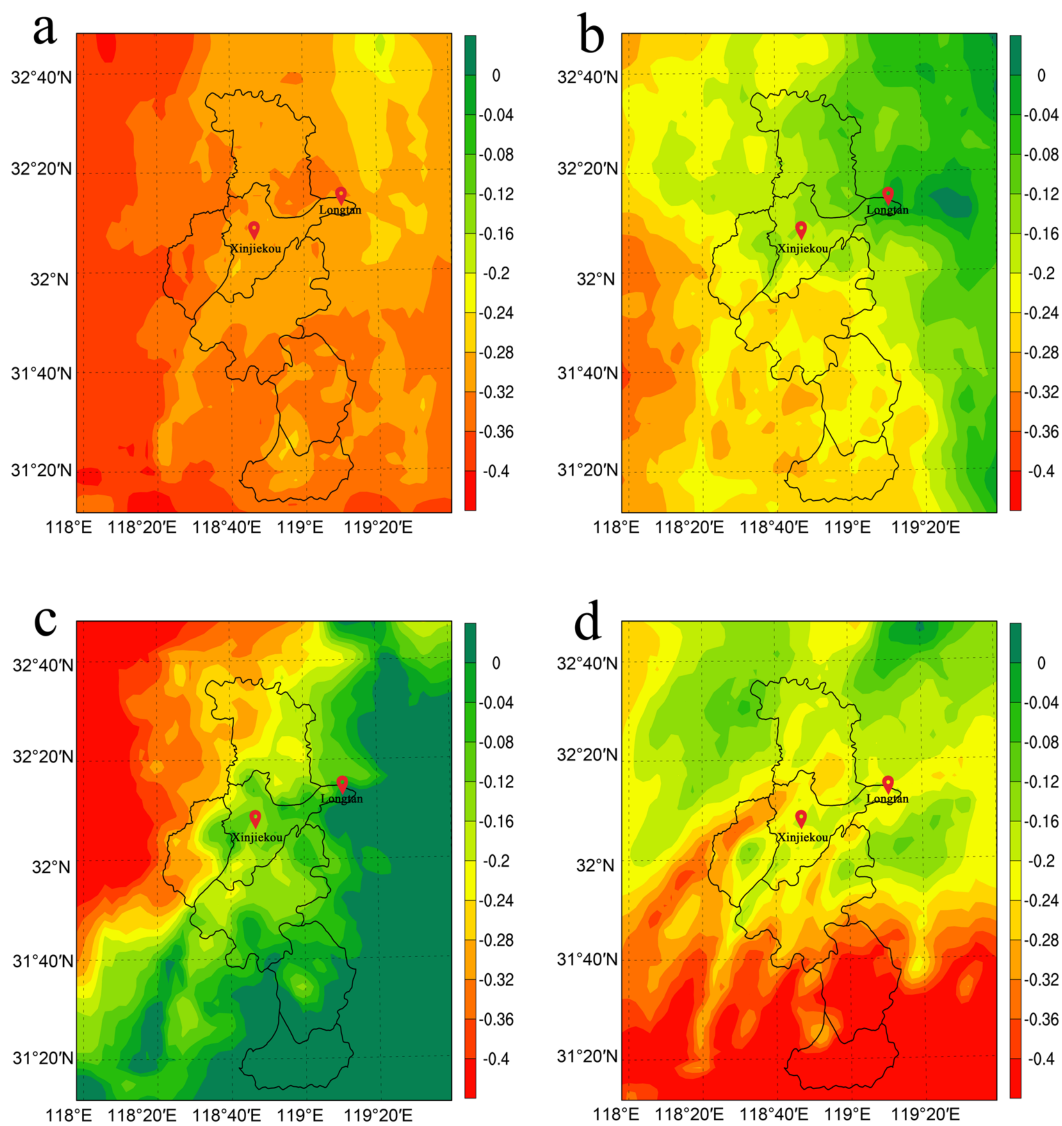

Figure 5. Monthly averaged surface temperature change Δ*T* (K) at a 2-m height due to $PM_{2.5}$ in (**a**) January; (**b**) April; (**c**) July; and (**d**) October, 2011. The maps were generated using NCAR Command Language (Version 6.2.0., https://www.ncl.ucar.edu, 2014).

Figure 3a shows a comparison of the observed and simulated UHI intensities for the station pair Beijige and Pukou for the four months of January, April, July, and October. The monthly averages of the UHI intensities were well captured by the model, as the averages are the same for model and observations (1 K, 0.7 K, 0.2 K and 0.4 K in January, April, July and October, respectively). The model simulation tends to underpredict the range of UHI intensity values on an hourly basis, especially in January. Figure 3b shows a quantitative comparison of the daily observed and simulated $PM_{2.5}$ concentrations at the urban site in Nanjing in 2011. Although the $PM_{2.5}$ levels in July and October are overpredicted by approximately 20 μg/m^3 and 15 μg/m^3, the daily variations were well simulated compared to the observations of the four months.

Figure 4 shows the horizontal distribution of the monthly averaged $PM_{2.5}$ concentrations over Nanjing from the output of the lowest model layer. In the urban centre, the average $PM_{2.5}$ concentration in 2011 was observed to be 40–50 μg/m^3 in the summer (June, July, August) and 80–90 μg/m^3 in the winter (December, January, February). In the suburban region, the average concentration was observed to be 30–40 μg/m^3 in the summer and 60–80 μg/m^3 in the winter, according to short-term observations[29]. The lower $PM_{2.5}$ concentrations in the summer can be explained as being the result of the increased amount of precipitation and better diffusion conditions induced by more instable atmosphere during the summer, resulting in increased surface $PM_{2.5}$ removal by wet deposition and vertical diffusion. Figure 4 shows that the simulations capture the seasonality of the $PM_{2.5}$ concentration. The simulated $PM_{2.5}$ concentration is highest in January (110–80 μg/m^3 in the urban centre) and lowest in July (100–70 μg/m^3 in the urban centre). Two other regions of high $PM_{2.5}$ concentrations are apparent near southwestern Nanjing: the cities of Maanshan and Wuhu. The high $PM_{2.5}$ concentrations of these two cities affect the southern suburban areas of Nanjing and do not impact the suburban stations of our numerical experiments.

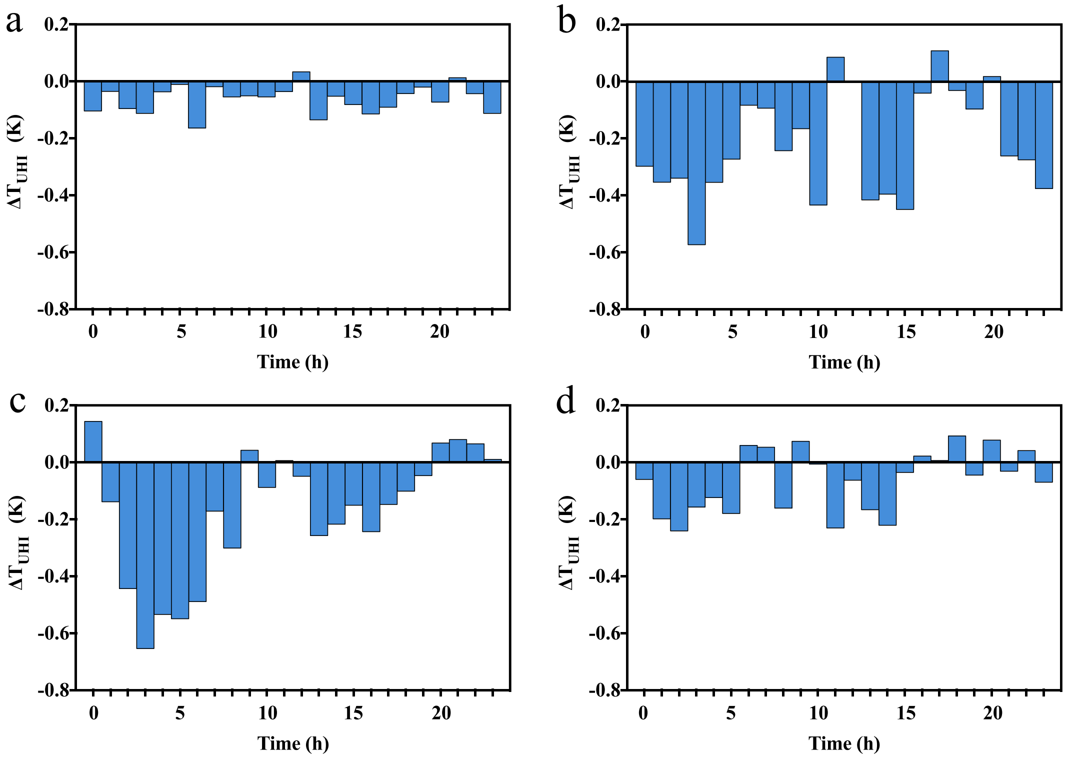

Figure 6. Monthly averages of the diurnal cycles of the simulated changes in UHI intensities due to $PM_{2.5}$ (ΔT_{UHI}) for (**a**) January, (**b**) April, (**c**) July, (**d**) October, 2011. The shaded bars indicate the values of ΔT_{UHI}. The figure was produced using Prism 6.

Figure 5 shows the horizontal distribution of the surface temperature differences caused by $PM_{2.5}$. Owing to the seasonal variation of the $PM_{2.5}$ concentration, the surface temperature change (ΔT) over the area is generally highest in January and lowest in July. However, to determine the impact of $PM_{2.5}$ on the UHI (quantified via ΔT_{UHI}), we need to compare the ΔT of the urban area to the ΔT of the suburban area, as a simple correlation with the $PM_{2.5}$ map cannot be expected. Aerosols both scatter and absorb solar radiation, thus cooling the surface. However, the simulated surface temperature is still dependent on other factors; when the aerosols cool the surface temperature, the atmosphere becomes more stable, which changes the moisture transport and results in cloud and precipitation feedbacks, which affect temperature again. Due to these complex feedbacks, the horizontal distribution of the surface temperature response is not always similar to the horizontal distribution of the $PM_{2.5}$ differences. However, the surface temperature gradient around the $PM_{2.5}$ source can be found in Figs 4 and 5.

Simulated $PM_{2.5}$ effects on the surface UHI. According to the observational results discussed in Section 3.1, the UHI intensity is weakened during the day as the $PM_{2.5}$ concentrations increase. From the simulations, we learn that the surface temperature cooling is indeed inhomogeneous across the domain (Fig. 5). Higher reductions of the surface temperature, as large as 0.3 K, were found in the urban centre, especially in July, while the reduction of the surface temperature was only 0.2 K in the suburban region.

Next, we quantified the diurnal variations of the simulated changes in the UHI intensities due to the presence of $PM_{2.5}$, ΔT_{UHI}. Negative values of ΔT_{UHI} correspond to weakened UHI intensities caused by the presence of $PM_{2.5}$. Figure 6 shows the diurnal cycle of the changes in the UHI intensities caused by those of $PM_{2.5}$ over the four different months. During the day, the surface temperature was reduced due to decreased solar radiation caused by the scattering and absorbing aerosols in both the urban and the suburban region. However, since the $PM_{2.5}$ loading of the urban region is consistently larger than that in the suburban region, the temperature decrease was larger in the urban region, which explains the decreased UHI intensity when $PM_{2.5}$ was included in the simulations. While ΔT_{UHI} is positive at a few points, the magnitudes of these points are small. Thus, the strengthening of the night-time UHI intensity caused by heavy pollution conditions seen in the observational data (Fig. 2) is not found in the simulation results (Fig. 6) because we do not separate the low, middle and high pollution days when calculating the monthly average diurnal UHI intensity changes.

Figure 6 also shows that the magnitude of the ΔT_{UHI} was larger in April and July than in January and October. Table 1 shows the monthly averaged T_{UHI} values with and without the $PM_{2.5}$ effects and the resulting ΔT_{UHI}. The seasonal variations of ΔT_{UHI} depend on both the available solar radiation and the differences of the $PM_{2.5}$ levels of the urban centre and the suburban area. Without the $PM_{2.5}$ effect, T_{UHI} mainly depends on solar radiation, which varies according to the seasons. As a result, T_{UHI} was highest in July and lowest in January. However, $PM_{2.5}$ obviously weakened the UHI intensity, and the differences of the $PM_{2.5}$ levels of the urban centre and the suburban area are larger in July (18.51 $\mu g/m^3$) than in January (15.86 $\mu g/m^3$). When including $PM_{2.5}$ in the simulations, T_{UHI}

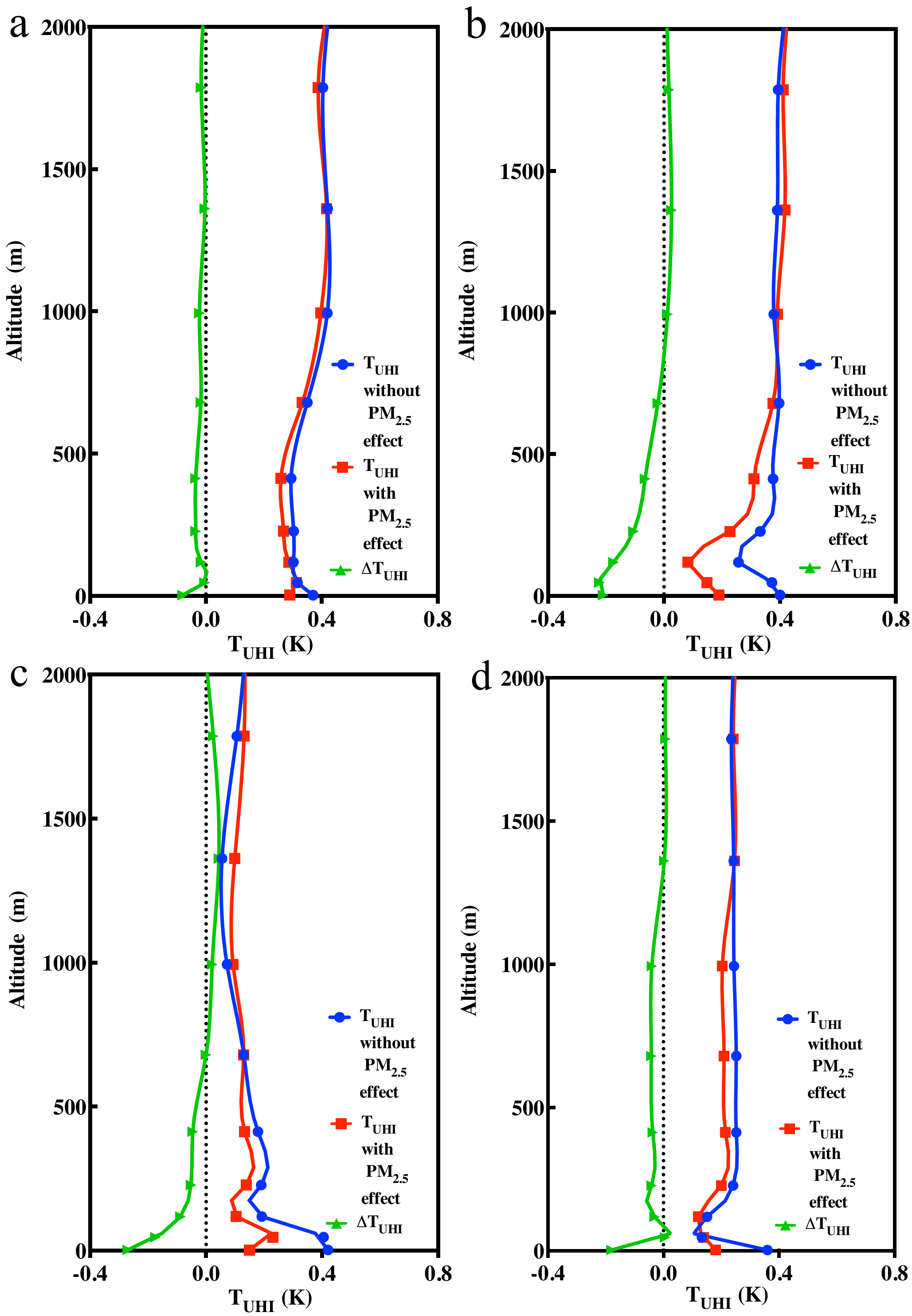

Figure 7. Monthly average T_{UHI} profile from 2 m to 2000 m in (**a**) January; (**b**) April; (**c**) July; (**d**) October. Blue, red and green lines indicate the UHI intensities without the $PM_{2.5}$ radiation forcing, with the $PM_{2.5}$ radiation forcing and the differences of the former two cases at different altitudes.

	January	April	July	October
T_{UHI} without the $PM_{2.5}$ effect (K)	0.37	0.40	0.42	0.36
T_{UHI} with the $PM_{2.5}$ effect (K)	0.29	0.19	0.15	0.18
ΔT_{UHI} (K)	**−0.08**	**−0.21**	**−0.27**	**−0.18**

Table 1. Monthly averaged values of T_{UHI} and ΔT_{UHI} at 2-m heights affected by $PM_{2.5}$.

	With $PM_{2.5}$ effect	January	April	July	Octo ber
Urban daily temperature range	Yes	6.95	10.95	8.71	7.98
Urban daily temperature range	No	7.04	11.47	9.81	8.05
Urban ΔT_{dr}	—	**−0.09**	**−0.52**	**−1.1**	**−0.07**
Suburban daily temperature range	Yes	6.94	10.68	8.45	8.04
Suburban daily temperature range	No	6.98	10.77	9.33	8.35
Suburban ΔT_{dr}	—	**−0.04**	**−0.09**	**−0.88**	**−0.31**

Table 2. Monthly variations of temperature daily ranges in 2011, Nanjing (K).

reached a lowest value of nearly 0.15 K in July and a highest value at nearly 0.3 K in January. In general, $PM_{2.5}$ contributed to the ΔT_{UHI} the most, with −0.27 K in July, and the least, with −0.08 K, in January, due to the seasonal variations of the $PM_{2.5}$ concentrations and solar radiation.

Simulated $PM_{2.5}$ effect on the UHI profile. While we have discussed changes in the UHI intensities near the surface caused by $PM_{2.5}$, the changes in temperature due to $PM_{2.5}$ also exist in higher layers. Figure 7 shows the vertical profiles of the UHI intensities with and without including the effects of $PM_{2.5}$, as well as the change due to $PM_{2.5}$. In the four months studied, the T_{UHI} values have similar vertical profiles, first declining from the surface up to 100 m, then increasing to a height of approximately 1000 m and remaining constant between 1000 m and 2000 m. This finding shows that the UHI intensity changes can be observed at well over 500 m[41]. The ΔT_{UHI} profile shows that $PM_{2.5}$ reduces the UHI intensity at lower altitudes, usually below 500–1000 m. For higher altitudes, the ΔT_{UHI} values approach zero in January and October. In April (Fig. 7b) and July (Fig. 7c), the ΔT_{UHI} values are larger than zero when the altitude is over 1000 m and decrease to zero at 2000 m. The UHI intensity was most weakened by $PM_{2.5}$ near the surface, but the weakening effect decreases with height. Therefore, the ΔT_{UHI} shown in Fig. 7b,c approach 0 K in the 600–700 m layer, with negative values below this height. The small positive values of ΔT_{UHI} shown in Fig. 7b,c above 600–700 m mean that the UHI intensity was intensified by as little as 0.03 K, which may be the result of the aerosol warming effect, which is caused by the absorption of solar radiation in the upper levels of the boundary layer. This phenomenon is dependent on the chemical composition and vertical distribution of $PM_{2.5}$, which should be addressed in more detail in a future study. This seasonal variation occurs because $PM_{2.5}$ is mainly limited to the boundary layer, and the top of the boundary layer is higher in the spring and summer than in the fall and winter.

$PM_{2.5}$ effect on the daily temperature range. The change of the daily temperature range (referred as ΔT_{dr} in following text) is a useful metric to demonstrate the effects of $PM_{2.5}$ in the urban centre and over the suburban area[42]. Table 2 shows the changes of the daily temperature ranges caused by $PM_{2.5}$ over the four months. In each month, $PM_{2.5}$ reduced the daily temperature range. Considering $PM_{2.5}$'s cooling effect during the day and its weak warming effect at night, the reduction in the daily temperature range is caused by both maximum temperature decreases and the minimum temperature increases, which is true in both the urban and the suburban regions. The magnitude of the ΔT_{dr} affected by $PM_{2.5}$ is larger in the urban centre than in the suburban region.

Conclusions

Our study reveals that fine particles weakened the UHI intensities during the day using observational analysis and numerical modelling. Based on observations, the UHI intensity can be reduced by up to 1 K under heavily polluted conditions. According to our simulations, $PM_{2.5}$ reduced the surface radiation and the surface temperature[22,27] by up to 0.3 K in the urban centre of Nanjing. The simulated $PM_{2.5}$ concentrations were higher in the urban centre than those in the suburban area for all four studied months, thus affecting the UHI intensities. The simulated $PM_{2.5}$ concentration differences between the urban and suburban sites were, on average, 15.86 $\mu g/m^3$, 20.42 $\mu g/m^3$, 18.51 $\mu g/m^3$, 16.73 $\mu g/m^3$ in January, April, July and October, respectively. The seasonal variations of the $PM_{2.5}$ differences over the four months are consistent with those of ΔT_{UHI}, where the UHI intensity is weakened less in January and October but more in April and July. The day-time UHI intensity reduction was strongest in July and weakest in January as both the $PM_{2.5}$ concentration differences between the urban and suburban areas and the incoming solar radiation varied across different seasons. The reduction mainly occurred at altitudes below 500–1000 m. The response of the UHI intensity to the $PM_{2.5}$ at night depended on the $PM_{2.5}$ load. The night-time UHI intensity was weakened when the pollution levels were low to medium but was strengthened when the pollution levels were high.

$PM_{2.5}$ also reduced the daily temperature ranges, according to the simulations. The daily temperature range values in the urban centre were greater than those in the suburban area for all four months, as was the reduction caused by $PM_{2.5}$.

The UHI intensity and daily temperature range are significant reference signals of the urban climate. We showed that $PM_{2.5}$ pollution reduces urban warming during the day but can intensify the warming at night when the pollution levels are high. Thus, pollution can mask the UHI effects, and pollution levels need to be considered when comparing the UHI intensities of different cities. In a future study, we will further investigate the impact of the $PM_{2.5}$ compositions, as the scattering and absorbing aerosols cause different radiative forcings.

References

1. Howard, L. The climate of London: deduced from meteorological observations made in the metropolis and at various places around it. Vol. 2 (Harvey and Darton, J. and A. Arch, Longman, Hatchard, S. Highley [and] R. Hunter, 1833).
2. Manley, G. On the frequency of snowfall in metropolitan England. *Quart. J. Roy. Meteor. Soc.* **84**, 70–72 (1958).
3. Chen, X.-L., Zhao, H.-M., Li, P.-X. & Yin, Z.-Y. Remote sensing image-based analysis of the relationship between urban heat island and land use/cover changes. *Remote. Sens. Environ.* **104**, 133–146 (2006).
4. Oke, T. R. *Boundary layer climates*. (Routledge, 2002).
5. Xia, X., Li, Z., Wang, P., Chen, H. & Cribb, M. Estimation of aerosol effects on surface irradiance based on measurements and radiative transfer model simulations in northern China. *J. Geophys. Res.* **112** D22 (2007).
6. Lin, C.-Y. *et al*. Urban heat island effect and its impact on boundary layer development and land–sea circulation over northern Taiwan. *Atmos. Environ.* **42**, 5635–5649 (2008).
7. Weng, Q. & Yang, S. Managing the adverse thermal effects of urban development in a densely populated Chinese city. *J. Environ. Manage.* **70**, 145–156 (2004).
8. Zhao, L., Lee, X., Smith, R. B. & Oleson, K. Strong contributions of local background climate to urban heat islands. *Nature.* **511**, 216–219 (2014).
9. Huang, L., Zhao, D., Wang, J., Zhu, J. & Li, J. Scale impacts of land cover and vegetation corridors on urban thermal behavior in Nanjing, China. *Theor. Appl. Climatol.* **94**, 241–257 (2008).
10. Jones, P. *et al*. Assessment of urbanization effects in time series of surface air temperature over land. *Nature.* **347**, 169–172 (1990).
11. Peterson, T. C. *et al*. Global rural temperature trends. *Geophys. Res. Lett.* **26**, 329–332 (1999).
12. Gough, W. & Rozanov, Y. Aspects of Toronto's climate: heat island and lake breeze. *Canadian Meteoro. Oceanogr. Soc. Bull.* **29**, 67–71 (2001).
13. Mohsin, T. & Gough, W. A. Trend analysis of long-term temperature time series in the Greater Toronto Area (GTA). *Theor. App. Climatol.* **101**, 311–327 (2010).
14. Parker, D. E. Urban heat island effects on estimates of observed climate change. *Wiley Interdisciplinary Reviews: Climate Change.* **1**, 123–133 (2010).
15. Agarwal, M. & Tandon, A. Modeling of the urban heat island in the form of mesoscale wind and of its effect on air pollution dispersal. *Appl. Math. Model.* **34**, 2520–2530 (2010).
16. Fallmann, J., Emeis, S. & Suppan, P. *Modeling of the Urban Heat Island and its effect on Air Quality using WRF/WRF-Chem – Assessment of mitigation strategies for a Central European city*. (Springer International Publishing, 2014).
17. Fallmann, J., Forkel, R. & Emeis, S. Secondary effects of urban heat island mitigation measures on air quality. *Atmos. Environ.* **125**, 199–211 (2016).
18. Sarrat, C., Lemonsu, A., Masson, V. & Guedalia, D. Impact of urban heat island on regional atmospheric pollution. *Atmos. Environ.* **40**, 1743–1758 (2006).
19. Kaufman, Y. J., Tanré, D. & Boucher, O. A satellite view of aerosols in the climate system. *Nature.* **419**, 215–223 (2002).
20. Nabat, P. *et al*. Direct and semi-direct aerosol radiative effect on the Mediterranean climate variability using a coupled regional climate system model. *Climate. Dyn.* **44**, 1127–1155 (2014).
21. Vogel, B. *et al*. The comprehensive model system COSMO-ART–Radiative impact of aerosol on the state of the atmosphere on the regional scale. *Atmos. Chem. Phys.* **9**, 8661–8680 (2009).
22. Im, U. *et al*. Summertime aerosol chemical composition in the Eastern Mediterranean and its sensitivity to temperature. *Atmos. Environ.* **50**, 164–173 (2012).
23. Booth, B. B. B., Dunstone, N. J., Halloran, P. R., Andrews, T. & Bellouin, N. Erratum: Aerosols implicated as a prime driver of twentieth-century North Atlantic climate variability. *Nature.* **484**, 228–232 (2012).
24. Schmidt, G. A., Shindell, D. T. & Tsigaridis, K. Reconciling warming trends. *Nat. Geos.* **7**, 158–160 (2014).
25. Solomon, S. *et al*. The persistently variable "background" stratospheric aerosol layer and global climate change. *Science.* **333**, 866–870 (2011).
26. Schult, I., Feichter, J. & Cooke, W. F. Effect of black carbon and sulfate aerosols on the global radiation budget. *J. Geophys. Res.* **102**, 30107–30117 (1997).
27. Wu, J. *et al*. Simulation of direct effects of black carbon aerosol on temperature and hydrological cycle in Asia by a Regional Climate Model. *Meteor. Atmos. Phys.* **100**, 179–193 (2008).
28. Zhuang, B. *et al*. Optical properties and radiative forcing of urban aerosols in Nanjing, China. *Atmos. Environ.* **83**, 43–52 (2014).
29. Wu, H. *et al*. Impact of aerosol on the urban heat island intensity in Nanjing. *Trans. Atmos. Sci.* **37**, 425–431 (2014).
30. Chang, C. et al. Urban heat islands in China enhanced by haze pollution. *Nat. Commun.* **7** (2016).
31. Grell, G. A. *et al*. Fully coupled "online" chemistry within the WRF model. *Atmos. Environ.* **39**, 6957–6975 (2005).
32. Skamarock, W. C. & Klemp, J. B. A time-split nonhydrostatic atmospheric model for weather research and forecasting applications. *J. Comput. Phys.* **227**, 3465–3485 (2008).
33. Hong, S.-Y., Noh, Y. & Dudhia, J. A new vertical diffusion package with an explicit treatment of entrainment processes. *Month. Weat. Rev.* **134**, 2318–2341 (2006).
34. Chou, M. D., Suarez, M. J., Liang, X. Z., Yan, M. H. & Cote, C. A Thermal Infrared Radiation Parameterization for Atmospheric Studies. *Max J* (2001).
35. Mlawer, E. J., Taubman, S. J., Brown, P. D., Iacono, M. J. & Clough, S. A. Radiative transfer for inhomogeneous atmospheres: RRTM, a validated correlated-k model for the longwave. *J. Geophy. Res.* **102**, 16663–16682 (1997).
36. Stockwell, W. R., Middleton, P., Chang, J. S. & Tang, X. The second generation regional acid deposition model chemical mechanism for regional air quality modeling. *J. Geophy. Res.* **95**, 16343–16367 (1990).
37. Ackermann, I. J. *et al*. Modal aerosol dynamics model for Europe: Development and first applications. *Atmos. Environ.* **32**, 2981–2999 (1998).
38. Schell, B., Ackermann, I. J., Hass, H., Binkowski, F. S. & Ebel, A. Modeling the formation of secondary organic aerosol within a comprehensive air quality model system. *J. Geophy. Res.* **106**, 28275–28293 (2001).
39. Guenther, Z. P. & Wildermuth, M. Natural volatile organic compound emission rate estimates for US woodland landscapes. *Atmos. Environ.* **28**, 1197–1210 (1994).
40. Guenther, A. B., Zimmerman, P. R., Harley, P. C., Monson, R. K. & Fall, R. Isoprene and monoterpene emission rate variability: model evaluations and sensitivity analyses. *J. Geophy. Res.* **98**, 12609–12617 (1993).
41. Bornstein, R. D. Observations of the urban heat island effect in New York City. *J. Appl. Meteo.* **7**, 575–582 (1968).
42. Kalnay, E. & Cai, M. Impact of urbanization and land-use change on climate. *Nature* **423**, 528–531 (2003).

Acknowledgements

This work was supported by the National Natural Science Foundation of China (91544230, 41575145, 41621005), the National Key Basic Research Development Program of China (2016YFC0203303, 2016YFC0208504,2014CB441203), and the EU 7th Framework Marie Curie Actions IRSES Project: REQUA (PIRSES-GA-2013-612671). We appreciate the Nanjing Meteorological Bureau for the temperature data and the Nanjing Environmental Monitoring Center for the $PM_{2.5}$ concentration data.We thank Prof. Xuhui Lee from Yale University for his useful comments.

Author Contributions

H.W. performed the numerical experiments and analysed the data. H.W. and T.W. conceived the research topic. H.W., T.W. and N.R. wrote the manuscript. P.L., M.L. and S.L. provided help for the numerical experiments.

Additional Information

Competing Interests: The authors declare that they have no competing interests.

Publisher's note: Springer Nature remains neutral with regard to jurisdictional claims in published maps and institutional affiliations.